

2

AD-A247 911



A Simple Cloud Reflectance Model for Ship Tracks in Clouds

DTIC
ELECTE
MAR 16 1992
S B D

R. A. Siquig
Forecast Guidance and Naval Systems Support Division
Atmospheric Directorate
Monterey, CA 93943-5006



Approved for public release; distribution is unlimited. Naval Oceanographic and Atmospheric Research Laboratory, Stennis Space Center, Mississippi 39529-5004.

02 3 13 084

92-06699



ABSTRACT

Under certain meteorological conditions ships may generate "tracks" in overlying marine stratus or stratocumulus clouds. These tracks are often not particularly evident to satellite sensors at visible wavelengths, but show up much more clearly at near infrared wavelengths, such as channel 3 (3.7 μm) of the Advanced Very High Resolution Radiometer (AVHRR) on NOAA polar-orbiting satellites. This phenomenon represents a potential naval intelligence technique, not only as a means to monitor and perhaps classify ships of other nations but also as a measure of environmental vulnerability of U.S. ships. A simple theoretical model was used as part of a ship track study to investigate effects of changes in microphysics and geometry on cloud reflectance at certain solar wavelengths. The model assumed a plane parallel homogeneous atmosphere of infinite extent and finite thickness, with Mie scattering and the delta-Eddington approximation for radiative transfer. The results were consistent with the theory that ship exhaust can increase the number density of smaller cloud droplets, which would lead to an increase in reflectance of incident solar radiation, especially at wavelengths near 3.7 μm .

Accession For	
NTIS GRA&I	<input checked="" type="checkbox"/>
DTIC TAB	<input type="checkbox"/>
Unannounced	<input type="checkbox"/>
Justification	
By _____	
Distribution/ _____	
Availability Codes	
Dist	Availent/or Special
A-1	

ACKNOWLEDGMENTS

The support of the sponsor, the Office of Naval Technology, Program Element 62435N, is gratefully acknowledged.

An M.S. thesis by Gary Mineart at the Naval Postgraduate School (NPS) served as the starting point for this study, and I am indebted to Mineart's thesis advisor, Professor Phil Durkee, for his help and encouragement. I also received generous help from Craig Motell and Rick Kohrs at NPS.

TABLE OF CONTENTS

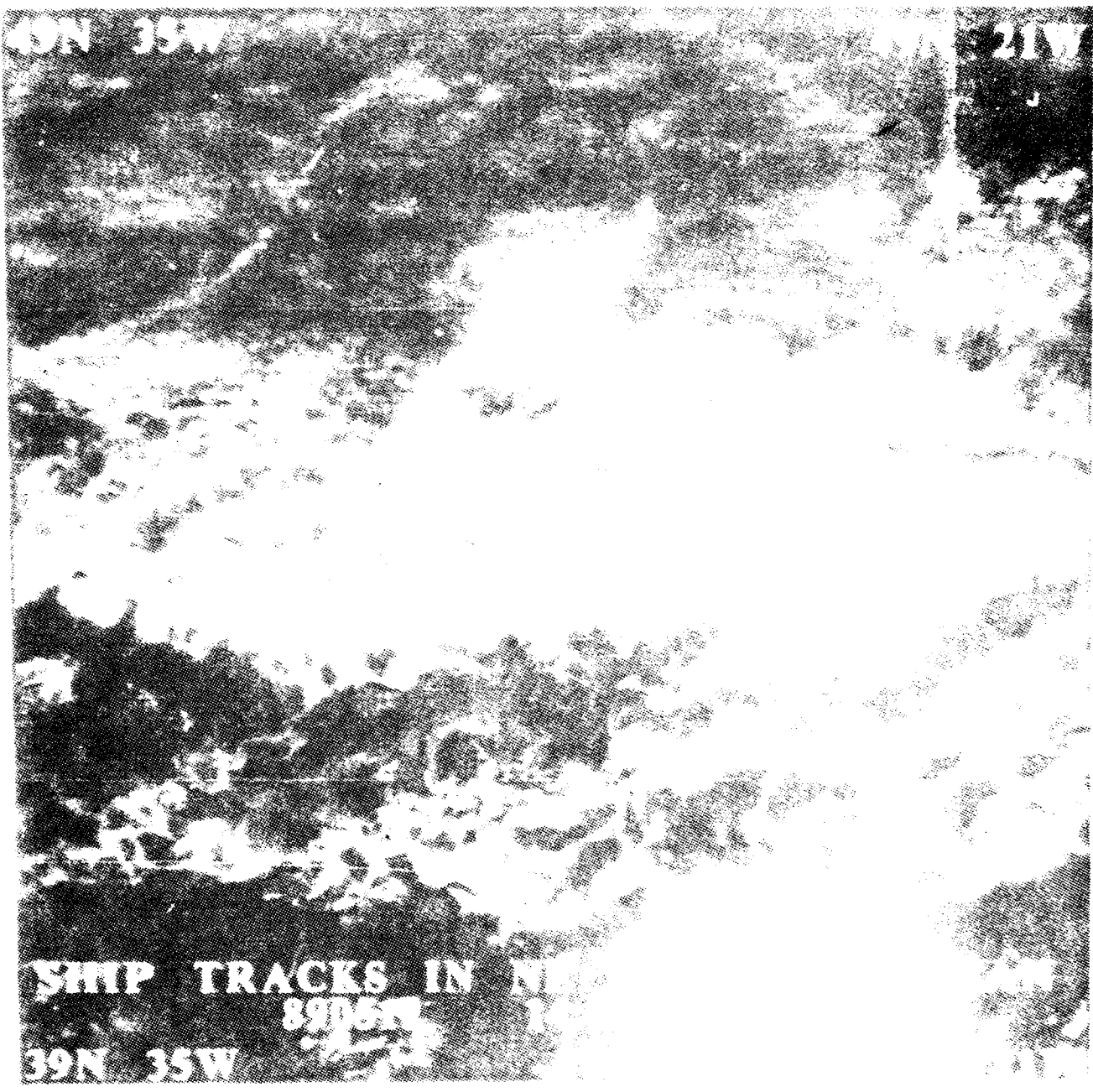
1.	INTRODUCTION	1
2.	RELEVANT MIE SCATTERING THEORY	3
2.1	Overview	3
2.2	Single Particle Mie Scattering	4
2.3	Polydispersion Mie Scattering	6
3.	RADIATIVE TRANSFER TREATMENT	8
3.1	Multiple Scattering and Radiative Transfer	8
3.2	Delta-Eddington Approximation	9
3.3	Additional Comments	10
4.	CHOICE OF PARAMETER VALUES	10
4.1	Approach	10
4.2	Parameter Values	11
5.	RESULTS	14
5.1	Overview	14
5.2	Scattering Optical Depth vs. Cloud Thickness	14
5.3	Single Scattering Albedo vs. Wavelength	16
5.4	Asymmetry Factor vs. Wavelength	18
5.5	Reflectance vs. Mode Radius	18
5.6	Reflectance vs. ELWC	18
5.7	Reflectance vs. Cloud Thickness	21
5.8	Dependence of Reflectance on Distribution	21
5.9	Dependence of Reflectance on Solar Zenith Angle	24
6.	CONCLUSIONS, FUTURE WORK	24
6.1	Conclusions	24
6.2	Future Work	27
6.2.1	N-layer model	27
6.2.2	Multi-channel correlations	29
6.2.3	Nonhomogeneous finite clouds	29
6.2.4	Polarization effects	29
6.2.5	Comparison with field data - satellite, aircraft	29
	REFERENCES	30

A SIMPLE CLOUD REFLECTANCE MODEL FOR SHIP TRACKS IN CLOUDS

1. INTRODUCTION

Clouds are a ubiquitous phenomenon, typically covering about fifty percent of the globe. They play a crucial role in determining the radiation budget of the earth and hence have a major effect on the dynamics of the atmosphere and the earth's climate. It has also been established that clouds are sensitive to anthropogenic effects, such as pollution, thus providing a link between man's activities and his environment. One intriguing naval phenomenon is the generation of "ship tracks" in clouds (Siquig et al., 1991). An example is given in Figure 1, which is a channel 3 (3.7 μm) image from the Advanced Very High Resolution Radiometer (AVHRR) on NOAA polar orbiter satellites showing a number of ship tracks. In AVHRR channel 1 (.63 μm), the tracks are much less evident. One possible explanation for ship tracks is that ship exhaust can increase the number of cloud condensation nuclei in overlying marine stratus or stratocumulus clouds, resulting in more but smaller cloud droplets which increase the cloud reflectance at near infrared (NIR) wavelengths relatively more than at visible (VIS) wavelengths (Coakley et al., 1987). Here a simple cloud reflectance model is used to explore this suggestion.

We start by observing that ship tracks usually occur in marine stratus or stratocumulus (st/sc) cloud decks which usually are some fraction of a kilometer thick. The observed tracks themselves seem to range in width from a few to about twenty kilometers. As a first approximation, then, a ship track can be considered as an infinite plane parallel homogeneous st/sc cloud layer with specified microphysics and thickness. This allows us to follow the approach of Mineart (1988), hereafter "Mineart," who demonstrated for marine stratocumulus clouds the sensitivity of reflectance to cloud microphysics and geometry. We have extended Mineart's analysis to include more data points and additional wavelengths, resulting in an



49N 35W

47N 21W

SHIP TRACKS IN NEAR

39N 35W

890579

increase in the data base of theoretical results by a factor of ten. Results were in basic agreement with the earlier work. The exhaust explanation for ship tracks is consistent with the model results, which show that a shift to smaller cloud droplet size has a greater impact proportionally on cloud reflectance at NIR than at VIS wavelengths.

Section 2 is a brief review of relevant Mie scattering theory, including scattering from a single homogeneous sphere and scattering from a polydispersion of homogeneous spheres with a specified size distribution. Section 3 reviews the delta-Eddington approximation to the radiative transfer equation for a plane-parallel homogeneous cloud layer of infinite extent. The choice of parameter values is described in Section 4. Representative results for reflectance as a function of several variables (wavelength, size distribution, mode radius, equivalent liquid water content, cloud thickness, and solar zenith angle) are presented in Section 5. Conclusions and suggestions for future work are given in Section 6.

2. RELEVANT MIE SCATTERING THEORY

2.1 Overview

Attenuation of radiation in the atmosphere occurs principally through absorption and scattering by atmospheric gases, cloud droplets and particulate matter. By confining our attention to atmospheric windows, the problem of atmospheric gases can be largely avoided, and for the wavelengths chosen, aerosols are not as important as cloud droplets because of their smaller scattering efficiencies. Thus, this simple model is reduced to a problem in cloud attenuation. To simplify the problem even further, we assume a plane parallel homogeneous cloud of infinite extent. The problem is then separated into several parts. In Section 2.2, scattering of electromagnetic (EM) unpolarized plane waves off a single homogeneous sphere is reviewed.

The results are extended in Section 2.3 to a polydispersion of homogeneous spheres with a specified droplet size distribution.

2.2 Single Particle Mie Scattering

Maxwell's equations can be used to generate a vector wave equation for electromagnetic waves in a given medium. For a homogeneous sphere with complex index of refraction m ,

$$m = v - ik \quad (1)$$

where the real and imaginary parts have a wavelength dependence, the incident and scattered wave solutions can be matched at the sphere boundary to arrive at the Mie scattering parameters for the far field. Stokes vectors (related to intensities) for the incident and scattered fields are related by a transformation matrix from which the scattering phase matrix is derived. A prominent feature of Mie scattering is its strong forward bias, a feature which will be fundamental for explaining many of the computational results.

It is convenient to introduce a dimensionless size parameter x , which is the ratio of the sphere's circumference to the radiation wavelength,

$$x = 2\pi r/\lambda \quad (2)$$

where

$$r = \text{sphere radius}$$

and

$$\lambda = \text{wavelength.}$$

For the two extremes $r \ll \lambda$ (Rayleigh scattering) and $r \gg \lambda$ (geometric optics), simple scattering formulae apply. For the intermediate regime, r of the order of λ , the correct solution (Mie) is quite complicated and is generally calculated only through computer programs. Since

cloud droplet sizes are comparable to the NIR wavelengths of interest (micrometer range), it was necessary to use such a program for this study (see, e.g., Wiscombe, 1980).

The three basic quantities that describe single particle scattering are

$Q_s(m,r)$ = scattering efficiency factor

$Q_e(m,r)$ = extinction efficiency factor

$P(m,r,\psi)$ = phase function for radius r ,

where ψ is the scattering angle relative to the incident direction. Basically, the efficiency factors are a measure of process cross-section of the particle relative to its geometric cross-section, while the phase function is a measure of the directionality of the scattering process. Figure 2 shows the complicated nature of Q_s , depending on the value of k .

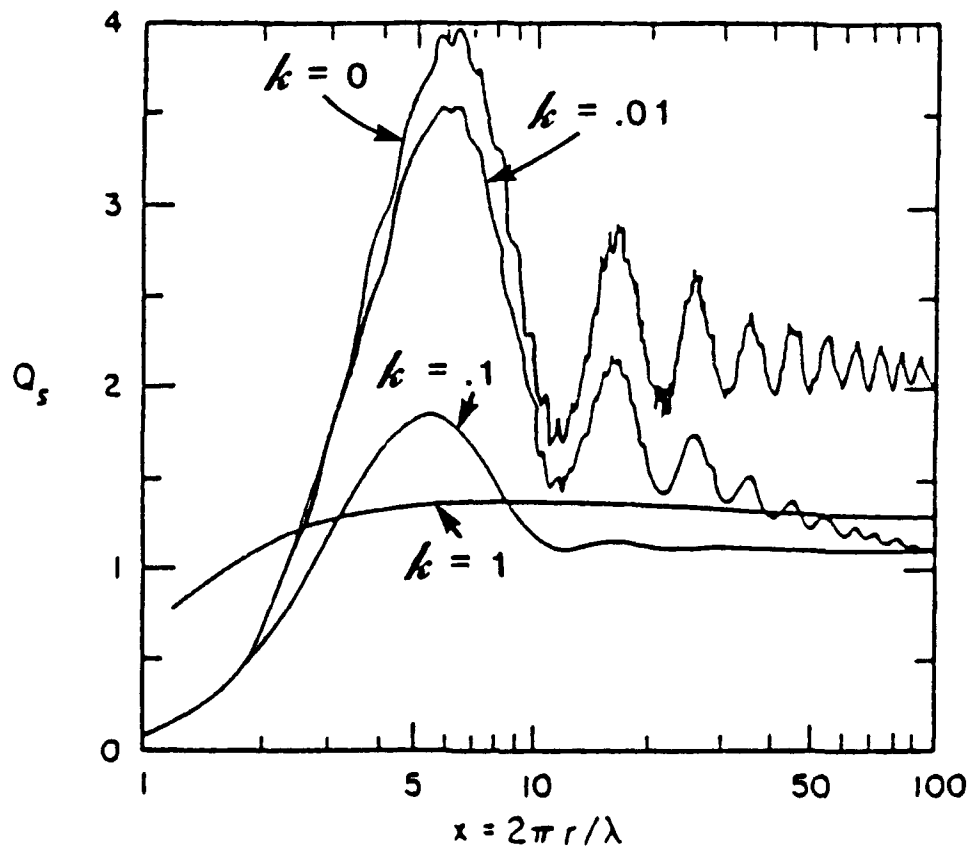


Figure 2. Mie scattering efficiency factor (Q_s): Illustrated as a function of the size parameter $x = 2\pi r/\lambda$. The real refractive index is 1.33, with results shown for four values of the imaginary part of the refractive index (after Hansen and Travis, 1974).

2.3 Polydispersion Mie Scattering

The Mie scattering analysis must be extended to a collection of homogeneous spheres in order to be applicable to a cloud model. Consider a polydispersion, i.e., a collection of scattering spheres of uniform physical properties, differing only in their size according to a known continuous size distribution. Furthermore, assume the particles are separated enough so that scattering off each particle is independent of scattering off the other particles. Then the intensities of scattering by various particles can be added without considering the phases of the scattered waves ("independent scattering").

By specifying a droplet size distribution $n(r)$ it becomes possible to generalize the above parameters to those appropriate for a polydispersion:

volume scattering coefficient

$$\sigma_s(\lambda) = \int_0^{\infty} \pi r^2 n(r) Q_s(m,r) dr \quad (3)$$

volume extinction coefficient

$$\sigma_e(\lambda) = \int_0^{\infty} \pi r^2 n(r) Q_e(m,r) dr \quad (4)$$

scattering phase function

$$P_s(m,\psi) = \frac{1}{\sigma_s(\lambda)} \int_0^{\infty} \pi r^2 n(r) Q_s(m,r) P(m,r,\psi) dr \quad (5)$$

In addition two other related parameters can be defined, the single scattering albedo

$$\omega_o = \frac{\sigma_s(\lambda)}{\sigma_a(\lambda)} \quad (6)$$

which is related to the probability that scattering will occur instead of absorption, and the asymmetry factor g

$$g = \langle \cos \psi \rangle = 1/2 \int_{-1}^1 P_s(m, \psi) \cos \psi d \cos \psi \quad (7)$$

which is related to the first moment of the phase function.

The actual details of the Mie derivation of $Q_s(m, r)$, $Q_a(m, r)$ and $P(m, r, \psi)$ are available in standard references, e.g., Kerker (1969) and Liou (1980); suffice it to say that the required parameters are x , m , and λ . With the specification of $n(r)$ instead of x , then the volume scattering coefficient σ_s , the single scattering albedo ω_o , and the asymmetry factor g can be used to characterize scattering off a small volume element of homogeneous spheres with size distribution $n(r)$. With suitable simplifying approximations, these three parameters are sufficient to describe the transfer of radiation within a cloud.

Before discussing in Section 3 the radiative transfer treatment, it might be instructive to point out why these three parameters are so useful. The volume scattering coefficient leads directly to the scattering optical depth $\delta_s(\lambda, z)$ for a physical distance z ,

$$\delta_s(\lambda, z) = \int_0^z \sigma_s(\lambda, z') dz' \quad (8)$$

which for a homogeneous medium is equivalent to

$$\delta_s(\lambda, z) = \sigma_s(\lambda) z \quad (9)$$

where δ_s is an optical measure of attenuation from scattering. The same physical distance z can have different values for δ_s , depending on σ_s . This fact will be useful later in interpreting the model results. The single scattering albedo is a measure of scattering versus absorption in the interaction of incident radiation with a small volume element. For example, $\omega_0 = 1$ means pure scattering with no absorption. Finally, the asymmetry factor is an integrated measure of the scattering directionality, where $g = 1$ means complete forward scattering, $g = 0$ means isotropic scattering, and $g = -1$ means complete backward scattering. Note that if an effective radius r_e is defined for the distribution such that

$$r_e = \frac{\int_0^{\infty} r^3 n(r) dr}{\int_0^{\infty} r^2 n(r) dr} \quad (10)$$

and if we define x_e

$$x_e = 2 \pi r_e / \lambda \quad (11)$$

then g approaches 0 as x_e becomes small (Rayleigh regime) and g approaches approximately .87 as x_e becomes large (geometric optics).

Thus, under certain conditions, these three parameters are sufficient to describe the integrated effects of all the radiation scattered from an extended cloud layer of finite thickness.

3. RADIATIVE TRANSFER TREATMENT

3.1 Multiple Scattering and Radiative Transfer

Most water clouds are optically thick, that is very few incident photons will escape scattering. Since the probability for multiple scattering is very high in a cloud, then the details of the phase function for single particle scattering are smoothed out in the multiple scattering

process, and only gross features of the phase function need to be specified, such as the asymmetry factor. Note, though, that if absorption becomes important through the wavelength dependence of the index of refraction, then the resultant scattered radiation retains more of its directional characteristics. This is because any scattered radiation cannot have entered too deeply into the cloud and still emerged, so it cannot have undergone too many scatterings. This connection between directionality of scattered radiation and the absorption properties of the cloud will be useful in explaining some of the model results.

Recall that σ_0 , ω_0 , and P_0 respectively determine 1) how much energy is lost from the incident beam in traversing a small volume element, 2) the probability that this energy will be lost by scattering or absorption, and 3) the probability that scattered energy will be sent into a particular direction. For a cloud composed of similar small volume elements, its effect upon incident radiation will also depend upon the geometry of the cloud and its orientation with respect to the incident beam. For hemispheric reflectance, the solar zenith angle will provide the cloud-beam orientation. The geometry problem can be simplified by choosing a homogeneous plane parallel layer of infinite extent. These assumptions reduce the complexity of the radiative transfer equation enormously and allow us to use the delta-Eddington approximation, described below. So our additional parameters are cloud thickness z and solar zenith angle (sza) θ_0 .

3.2 Delta-Eddington Approximation

Most solutions to specific problems in radiative transfer require complex computer implementation. For our simple model a major simplification can be made, namely that the radiance can be described as a simple two-term expansion (Eddington approximation - see Shettle and Weinman, 1970). This results in straight-forward expressions for the reflectance off an infinite homogeneous plane-parallel cloud layer. The only input required is solar zenith angle,

asymmetry factor, scattering optical depth and single scattering albedo. This approximation can be improved by exploiting the significant forward peak in the scattering phase function. If the forward peak is approximated by a Dirac-delta function and the phase function by a two term expansion, then the resultant delta-Eddington approximation is equivalent to the Eddington approximation with transformed ω_0 , g , and δ_0 (Joseph et al., 1976). Thus the simple Eddington expressions for reflectance can be used with slight modification, vastly reducing the computational burden.

3.3 Additional Comments

We have seen that specifying the droplet composition m , size distribution $n(r)$, and wavelength λ allow us to determine the scattering optical depth δ_0 , single scattering albedo ω_0 , and asymmetry factor g . These, in turn, allow us to calculate hemispheric reflectance, given cloud thickness and solar zenith angle. We have assumed perfect transmission above the infinite cloud layer because of the window regions in the EM spectrum we are using. The attenuation coefficient of aerosols above the cloud is small compared to that for the cloud droplets, and also the water vapor content above the cloud dies off rapidly.

4. CHOICE OF PARAMETER VALUES

4.1 Approach

Our interest is in the effect of cloud microphysics (droplet size distribution and equivalent liquid water content (ELWC)) and geometry (cloud thickness) on measured reflectance values in atmospheric transmittance windows. To facilitate comparison with Minnert's work and extend its analysis, we have used his choice of mode radii, distributions, wavelengths, ELWC, cloud thicknesses, and solar zenith angles while adding extra values.

4.2 Parameter Values

The following wavelengths were chosen: .63, 1.6, 2.3, and 3.7 μm . The first and last are channels on the AVHRR and were used by Mineart. The other two are possible channels on future satellites. All these wavelengths are in atmospheric windows.

A modified gamma distribution as discussed in Deirmendjian (1969) was used to model droplet size distribution,

$$n(r) = Ar^\alpha e^{-\frac{\alpha}{\gamma} \left(\frac{r}{r_c}\right)^\gamma}, \quad (12)$$

where A , α , γ , r_c are positive and real and α is an integer. Note that $n(0) = 0$ and $n(\infty) = 0$ and that $n(r) = \text{maximum}$ at $r = r_c$, the mode radius. The distribution $n(r)$ gives the number density of particles within a small radius range. The total number density of particles is given by N ,

$$N = \int_0^\infty n(r) dr, \quad (13)$$

from which it is clear that A depends on N . The three distributions used by Mineart were

DISTRIBUTION	α	γ
D1	2	1.19
D2	5	2.41
D3	5	1.30

The values chosen for r_c were 4, 6, 8, 10, and 12 μm to bracket expected values for marine stratocumulus clouds, for which in situ droplet data were available. Mineart used the values 4 and 8 for r_c . For ELWC the following values were used: .2, .4, .6, and .8 gm/m^3 . Mineart used the values .4 and .8.

By specifying ELWC it was necessary to calculate the corresponding values for A. This was done by recognizing that

$$\text{ELWC} = \delta V = E \quad (14)$$

where

$$\delta = \text{density of water} = 10^6 \text{ gm/m}^3$$

$$V = \text{total droplet volume}$$

$$= \int_0^{\infty} \frac{4}{3} \pi r^3 n(r) dr. \quad (15)$$

It is straightforward to show that

$$A = \frac{\gamma \left(\frac{\alpha}{\gamma}\right)^{\frac{\alpha-4}{\gamma}}}{\frac{4}{3} \pi r_c^{\alpha+4} \Gamma\left(\frac{\alpha+4}{\gamma}\right) \rho} 10^{12} E, \quad (16)$$

where Γ is the normal gamma function. Typical curves for D1, D2, and D3 are shown in Figure 3, taken from Minuart. D3 may be considered as a typical droplet size distribution for marine stratocumulus clouds, D2 is a narrow peaked distribution, and D1 is a broad distribution. These distributions will be used to examine the effect of distribution shape on reflectance values.

The values of cloud thickness chosen were those used by Minuart : 10, 25, 50, 100, 250, 500, and 750 m. The solar zenith angle values used were also those of Minuart : 30, 45, and 60 degrees.

Figure 4 is a schematic of the scattering process being modeled.

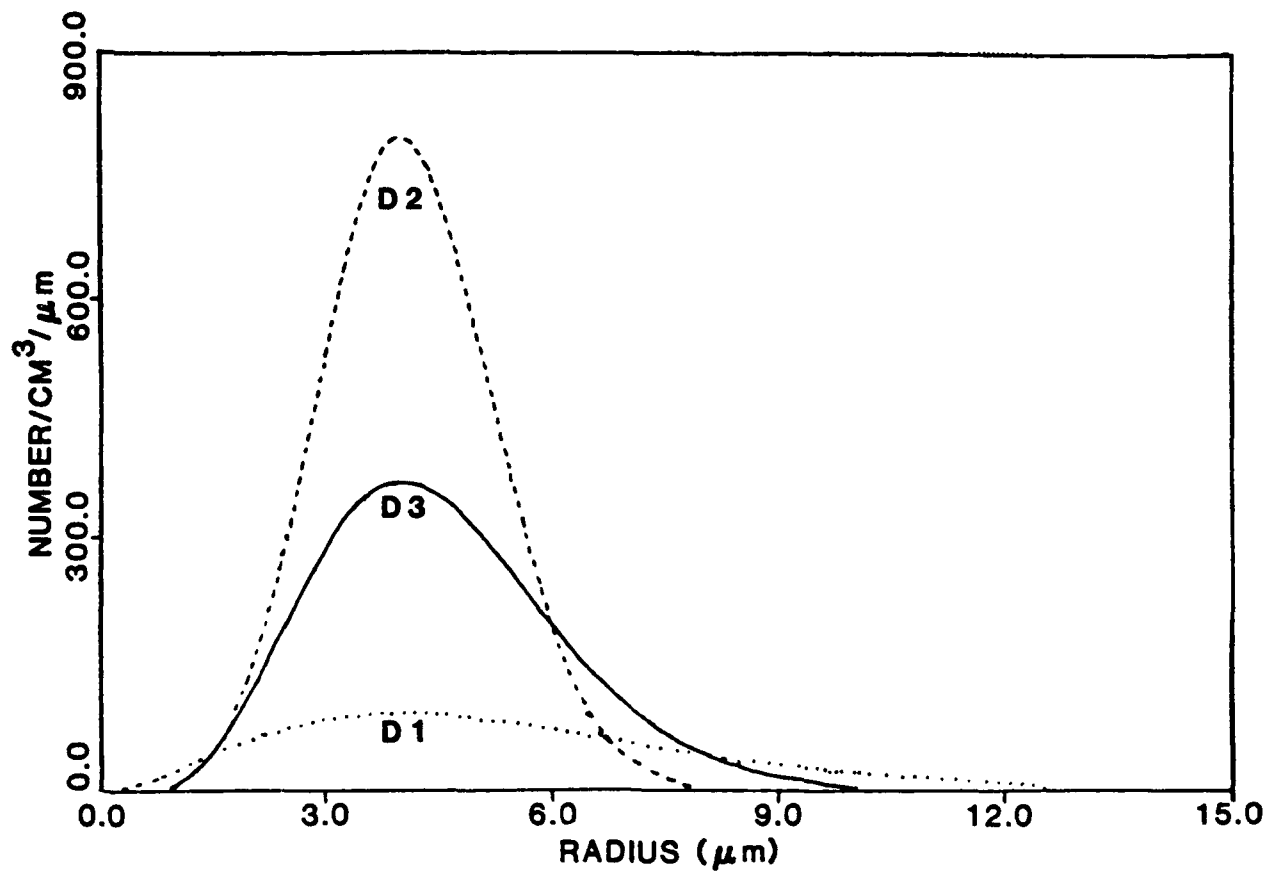


Figure 3. Droplet Size Distributions (after Mineart, 1988). The mode radius is 4 μm , and ELWC = .8 gm/m^3 .

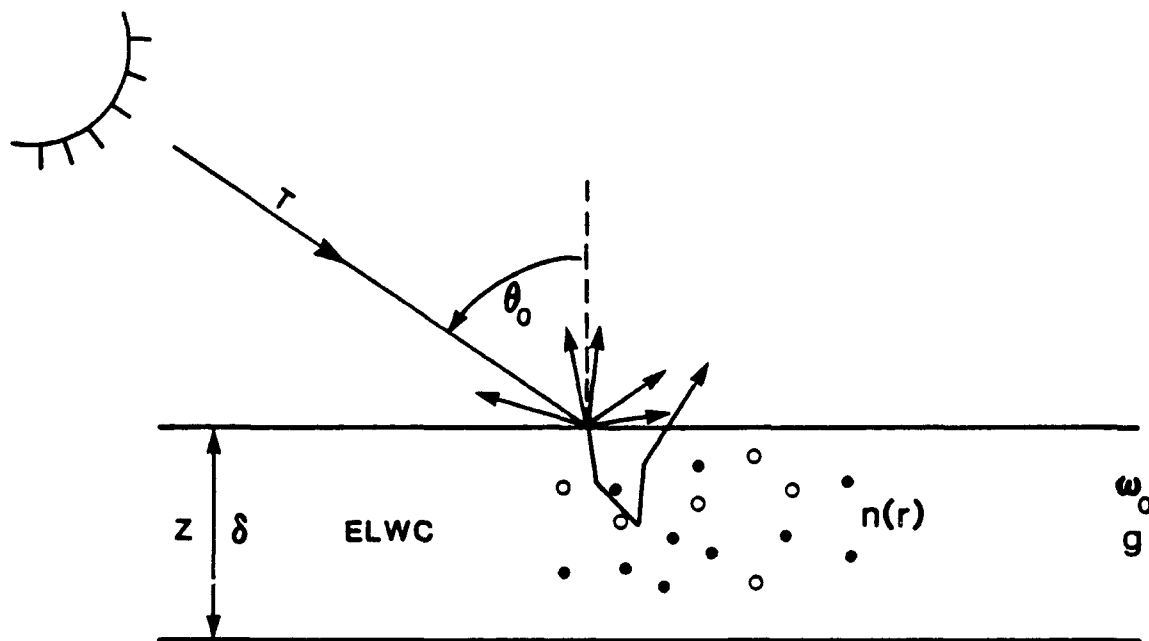


Figure 4. Schematic of cloud layer scattering.

5. RESULTS

5.1 Overview

The resulting data base of hemispheric reflectance as a function of wavelength, distribution, mode radius, ELWC, cloud thickness, and solar zenith angle consisted of 5040 entries, an increase by a factor of ten of Mineart's published results. Representative results will be presented here.

The addition of two more wavelengths, three more mode radii, and two more values for ELWC provide a more complete basis for asserting that an NIR channel could provide an indicator of cloud microphysical conditions. Furthermore, wavelengths at 1.6 and 2.3 μm also look promising for this purpose in addition to 3.7 μm as identified by Mineart. The shorter wavelengths have the advantage of greater energy in the incident solar spectrum and higher reflectance values, thus enhancing satellite sensor performance. Combining the results of several NIR channels may provide a more powerful tool than a single channel alone. Consistent with the earlier results, VIS wavelengths (.63 μm) are more suited to characterizing cloud geometry (thickness) than microphysics.

5.2 Scattering Optical Depth vs. Cloud Thickness

Figure 5 shows that for this homogeneous model scattering optical depth increases linearly with thickness as expected. The effect of increasing mode radius is to decrease optical depth. This may be explained by considering the effective radius for the distribution, r_e . The scattering optical depth has the dependence

$$\delta_s \sim N\pi r_e^2, \quad (17)$$

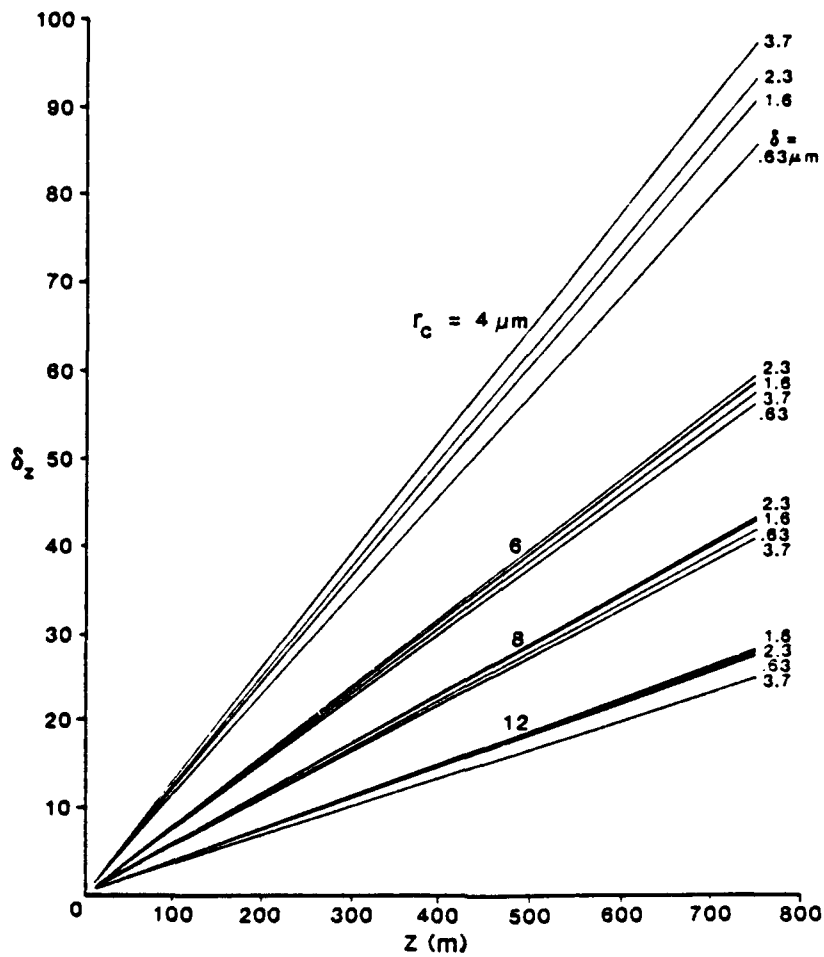


Figure 5. Scattering Optical Depth (δ_z) vs. Cloud Thickness (z). For ELWC = .4 gm/m³ and the D3 distribution. The four families of curves are labeled by mode radius and within each family the curves are distinguished by wavelength.

where for a fixed ELWC

$$N = \frac{ELWC}{\rho \frac{4}{3} \pi r_c^3} \quad (18)$$

Therefore,

$$\delta_s = \frac{1}{r_c} \quad (19)$$

indicating that if effective radius alone is increased, then scattering optical depth will decrease.

Note that it is straightforward to show that

$$r_e = r_c \left(\frac{\gamma}{\alpha} \right)^{1/\gamma} \frac{\Gamma\left(\frac{\alpha+4}{\gamma}\right)}{\Gamma\left(\frac{\alpha+3}{\gamma}\right)}, \quad (20)$$

so that r_e and r_c are related by a constant for a given distribution, so the above result applies also for the mode radius.

Increasing the wavelength may either increase or decrease the slope of the optical depth vs. thickness curve, depending on the mode radius. For our homogeneous approximation, optical depth is linearly related to the volume scattering coefficient given by equation 3; therefore, this effect is probably due to the oscillatory nature of the Mie scattering efficiency factor as a function of x and index of refraction (which has a wavelength dependence).

From equation 16, we see that A scales as ELWC and therefore so does σ_s , and hence also δ_s .

5.3 Single Scattering Albedo vs. Wavelength

Figure 6 shows that as wavelength increases the single scattering albedo decreases. This is a consequence of the generally greater absorption at the longer wavelengths, which is a result of the larger imaginary part of the index of refraction for water at the longer wavelengths. For a given wavelength, as mode radius increases, single scattering albedo decreases (if the wavelength is long enough). Note that ω_0 is more sensitive to changes in r_c at the longer wavelengths.

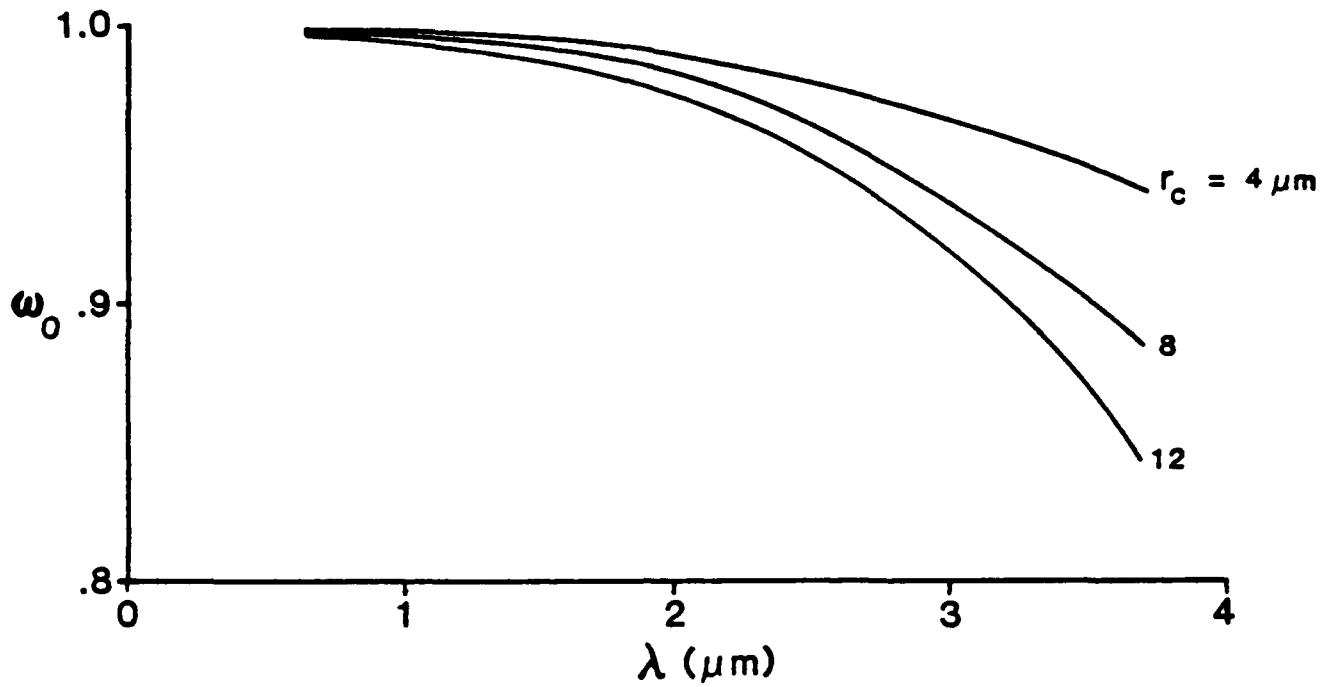


Figure 6. Single Scattering Albedo vs. Wavelength. For ELWC = .4 gm/m³ and the D3 distribution.

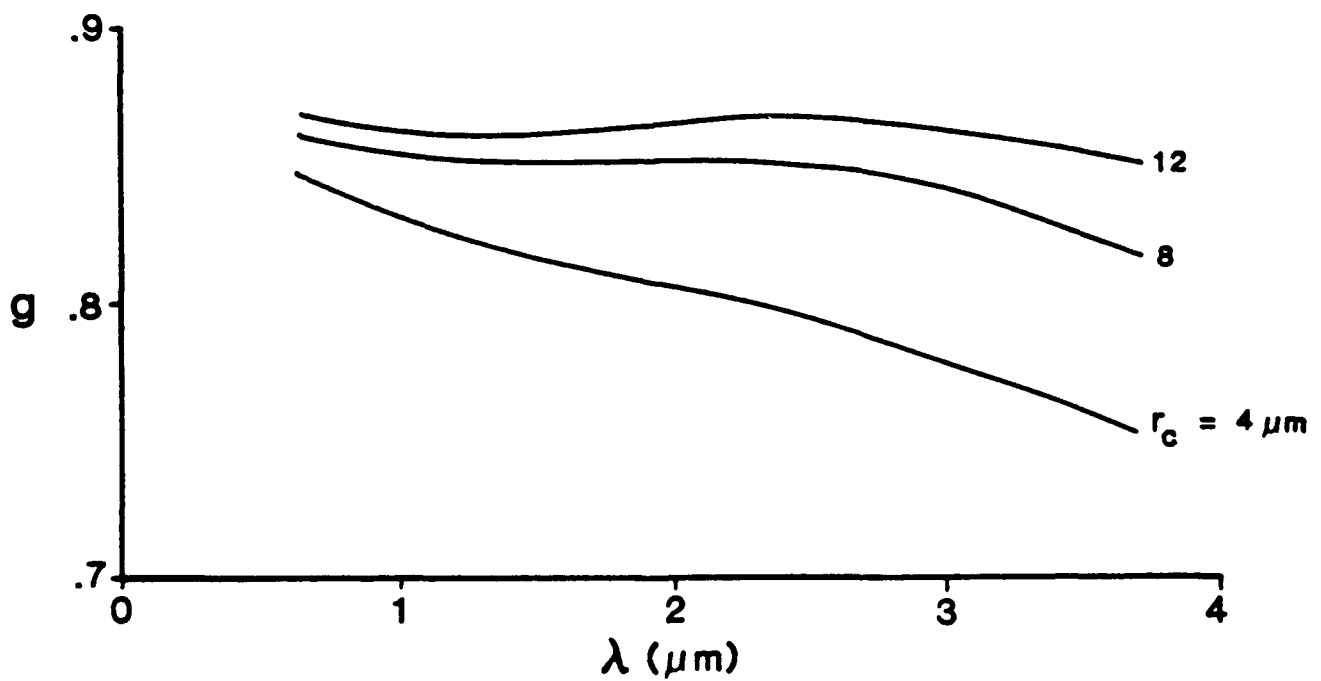


Figure 7. Asymmetry Factor vs. Wavelength. For ELWC = .4 gm/m³ and the D3 distribution.

5.4 Asymmetry Factor vs. Wavelength

Figure 7 shows that g does not have a simple monotonic behavior with respect to wavelength, depending on mode radius. This makes it harder to generalize about the computational results on the basis of the behavior of g . There does seem to be a tendency for g to decrease as wavelength is increased, i.e., as absorption is increased. For a given wavelength, g increases as mode radius increases, indicating increased forward scattering. This effect is more pronounced for the longer wavelengths.

5.5 Reflectance vs. Mode Radius

Figures 8a through 8d show clearly that 1) reflectance decreases as mode radius increases; 2) reflectance decreases as wavelength increases; 3) reflectance increases as ELWC increases, with this effect being less at the longer wavelengths; and 4) reflectance increases as cloud thickness increases, with this effect being less at the longer wavelengths. The latter two points are better described in later figures. For a given ELWC, as r_c increases, the number of droplets/unit volume must decrease. Therefore, for a given ELWC fewer but larger particles have less reflectance than more but smaller particles. One reason is that the larger particles tend to have more forward and less backward scattering. The second point above is primarily due to the increased absorption at the longer wavelengths.

5.6 Reflectance vs. ELWC

Figures 9a through 9d show that 1) in general reflectance increases as ELWC increases; 2) this effect is less pronounced at the longer wavelengths; 3) at any wavelength reflectance seems to saturate beyond a certain value for ELWC; 4) reflectance decreases as wavelength increases; 5) reflectance increases as cloud thickness increases, up to a point; and 6) reflectance decreases as mode radius increases. The first point simply means that at fixed r_c an increase in ELWC means an increase in the number of particles, and therefore more incident radiation is

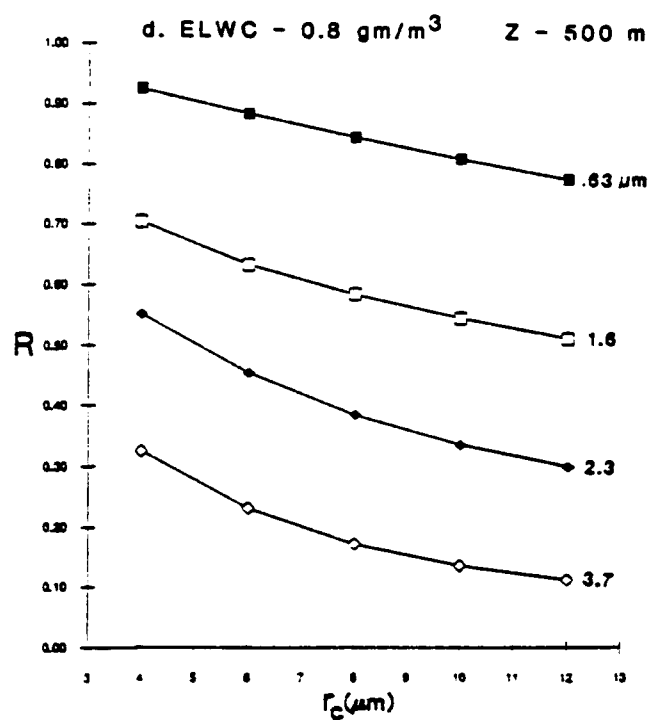
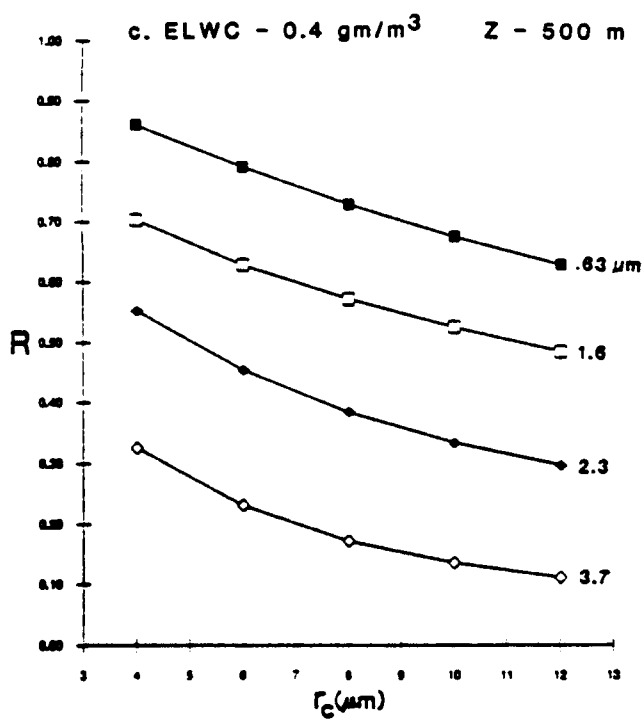
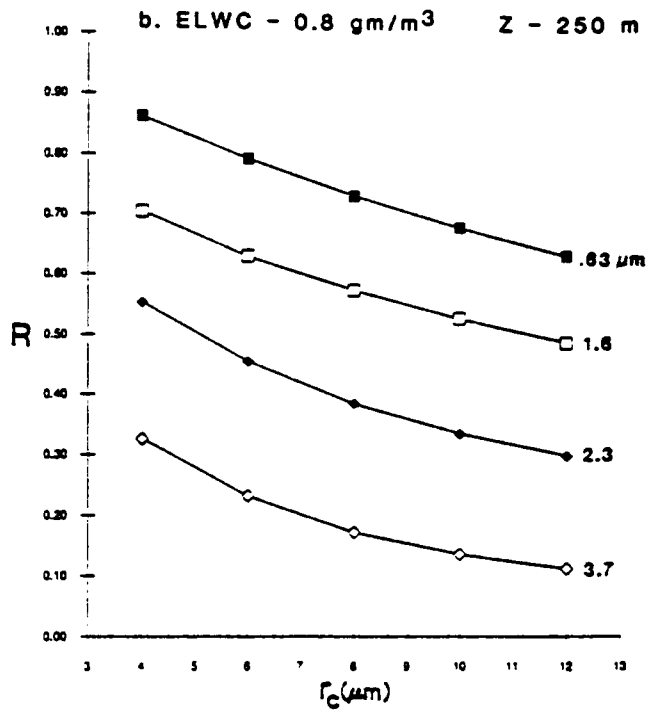
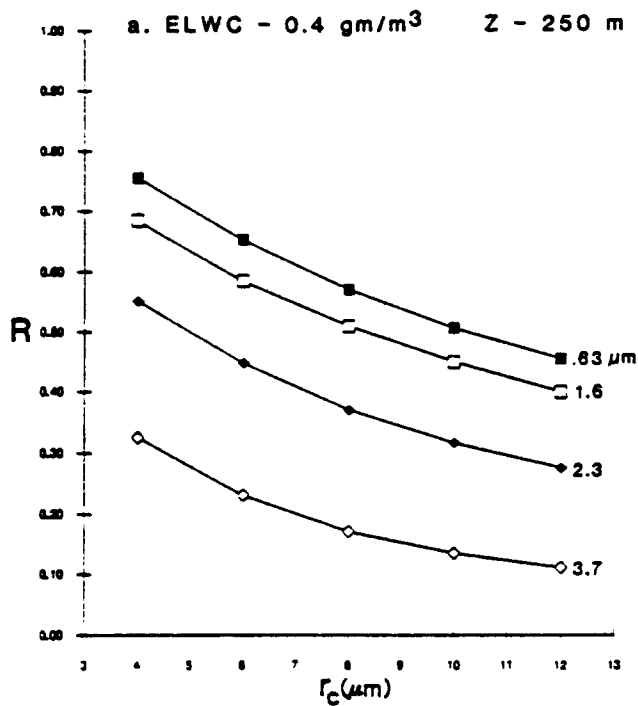


Figure 8. Reflectance vs. Mode Radius. For all cases the distribution is D3 and $\theta_0 = 45^\circ$. ELWC and cloud thickness vary as indicated. The curve symbols for the different wavelength values are used consistently in the following figures.

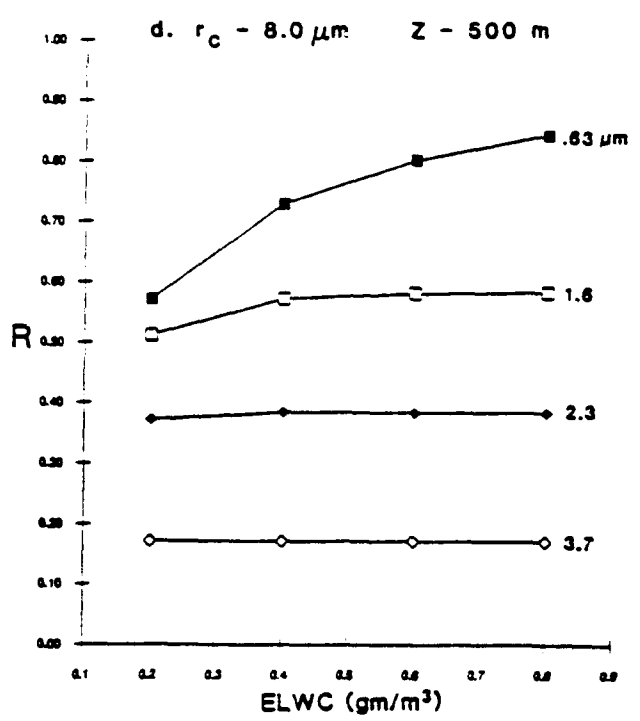
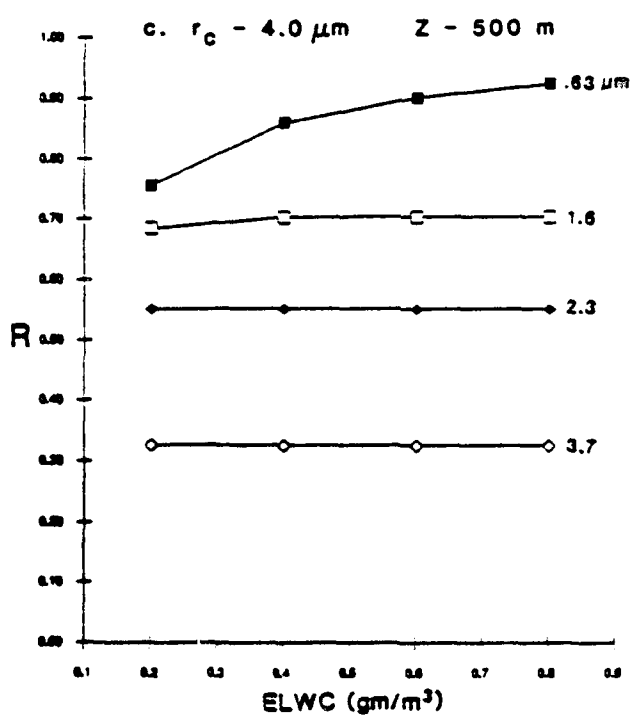
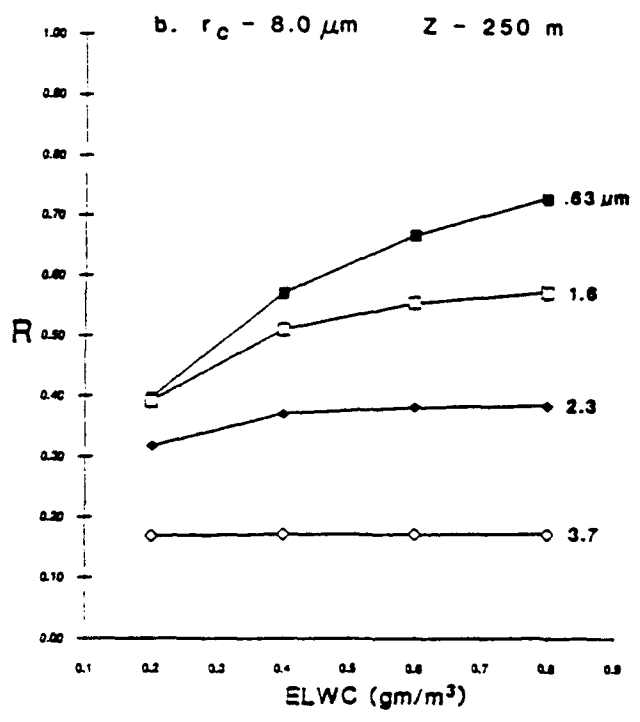
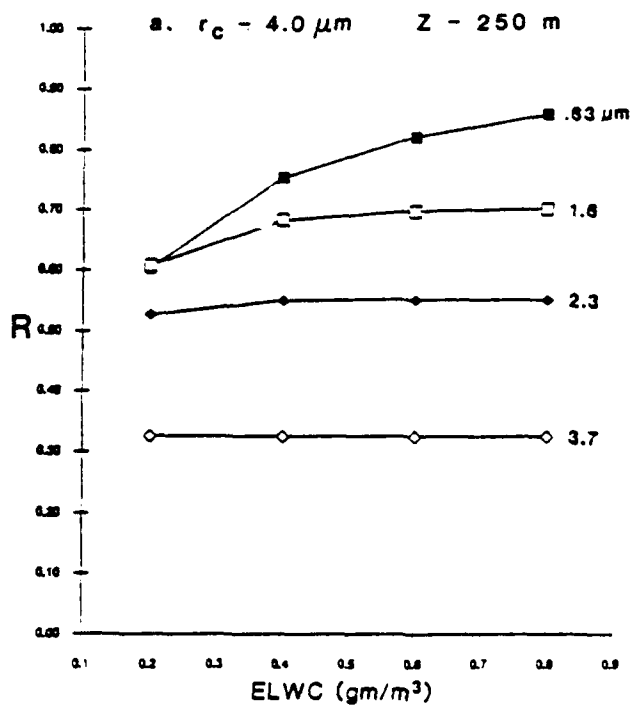


Figure 9. Reflectance vs. ELWC. For all cases the distribution is D3 and $\theta_0 = 45^\circ$. Mode radius and cloud thickness vary as indicated.

reflected. The second point is due to the increased importance of absorption at the longer wavelengths. The third and fifth points are best discussed in terms of optical depth. When the optical depth of the cloud exceeds a certain value, it may as well be infinite; increasing it no longer has any effect on reflectance. Optical depth (recall Figure 5) can depend on physical thickness, wavelength (through the effect of absorption on σ_s) and ELWC. As previously discussed the fourth point can be explained by the increased absorption at the longer wavelengths. The last point was explained in the first set of figures.

5.7 Reflectance vs. Cloud Thickness

Figures 10a through 10d show that 1) up to a certain point reflectance increases as thickness increases; 2) reflectance decreases as wavelength increases; 3) reflectance decreases as mode radius increases; 4) up to a point reflectance increases as ELWC increases; and 5) the cloud thickness at which reflectance saturates decreases as wavelength increases or as mode radius decreases. The first and fourth points have been explained from the point of view of optical depth. The second point has been explained by greater absorption at longer wavelengths. The third point is due to fewer scatterers at a given ELWC. The first part of the fifth point is due to greater absorption at longer wavelengths, allowing a thinner cloud to reach saturation for reflectance. The second part of the fifth point is because more scatterers/unit volume means an increase in optical depth for a given physical thickness.

5.8 Dependence of Reflectance on Distribution

Figure 11 shows that reflectance is greatest for the D2 distribution, followed by D3 and then D1. D2 is a narrow peaked distribution, D1 has a broad peak, and D3 is intermediate. From equation 20 one can calculate the ratio of effective radius to mode radius. For the D2, D3, and D1 distributions this ratio is 1.17, 1.42, and 2.13 respectively. Thus, the dependence of

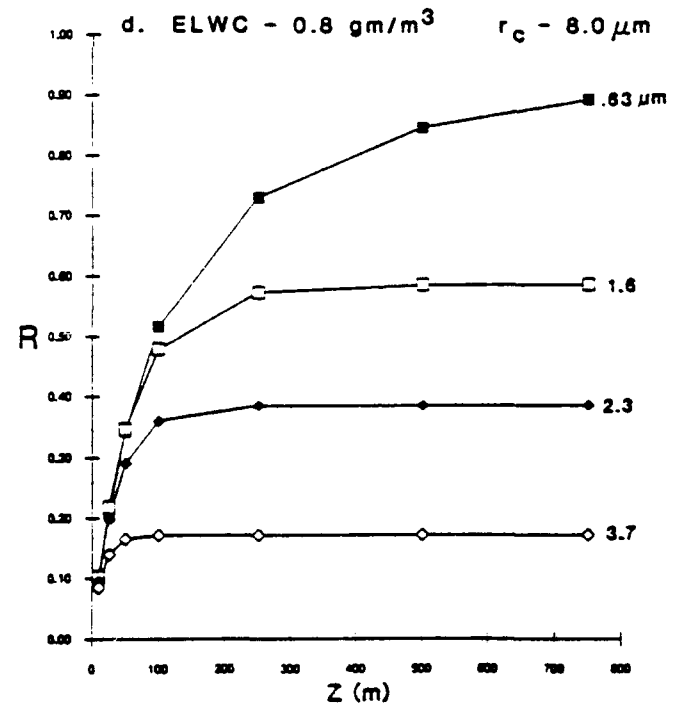
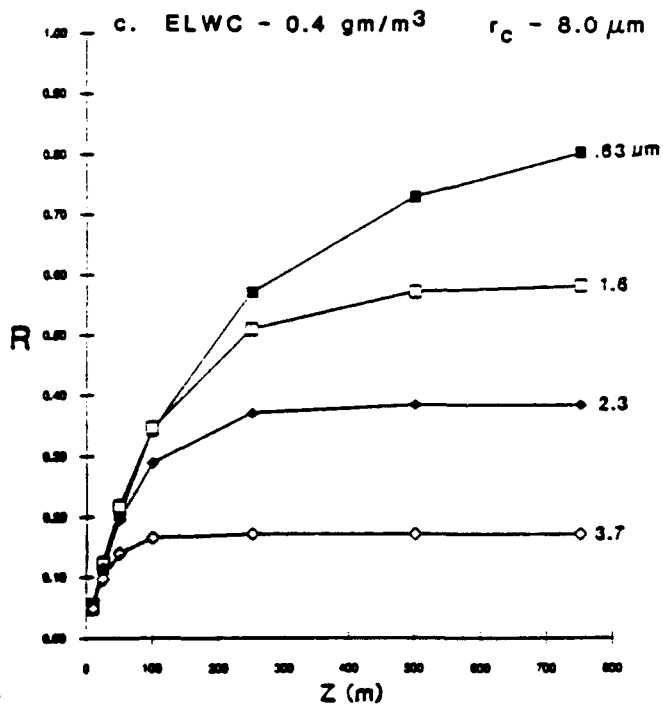
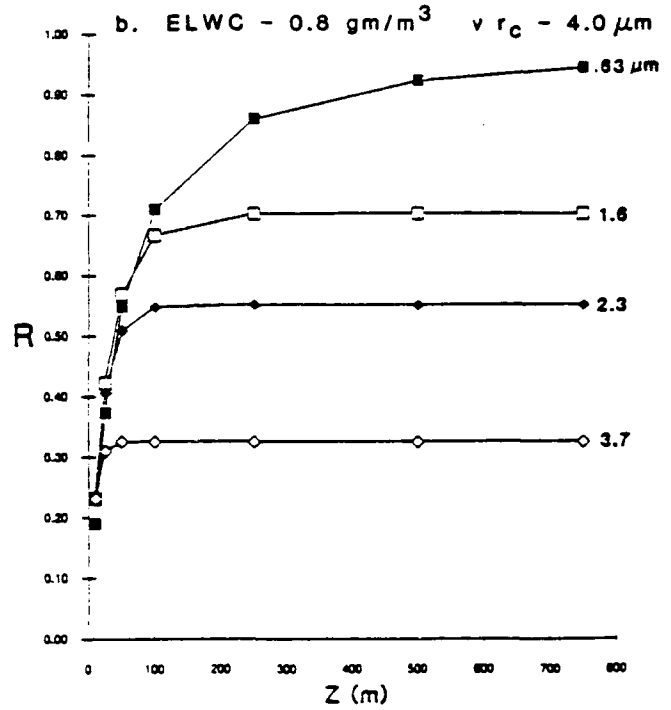
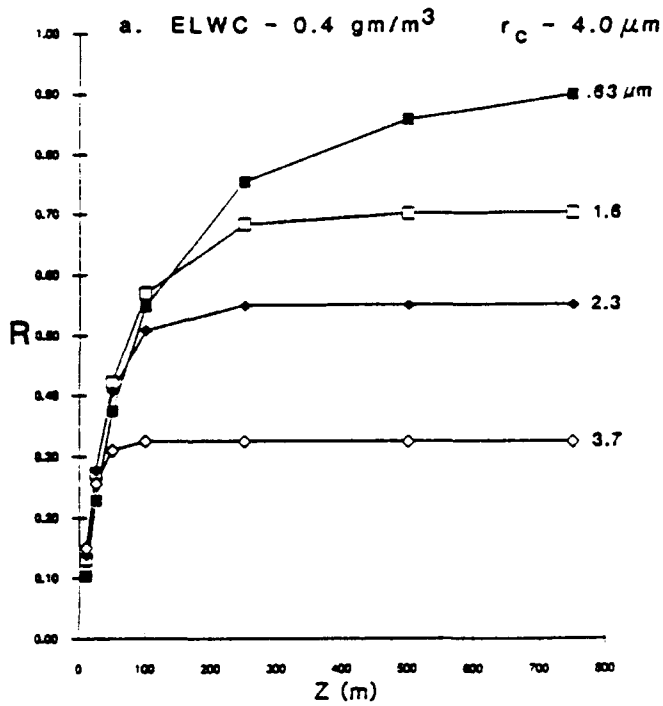


Figure 10. Reflectance vs. Cloud Thickness. For all cases the distribution is D3 and $\theta_0 = 45^\circ$. ELWC and mode radius vary as indicated.

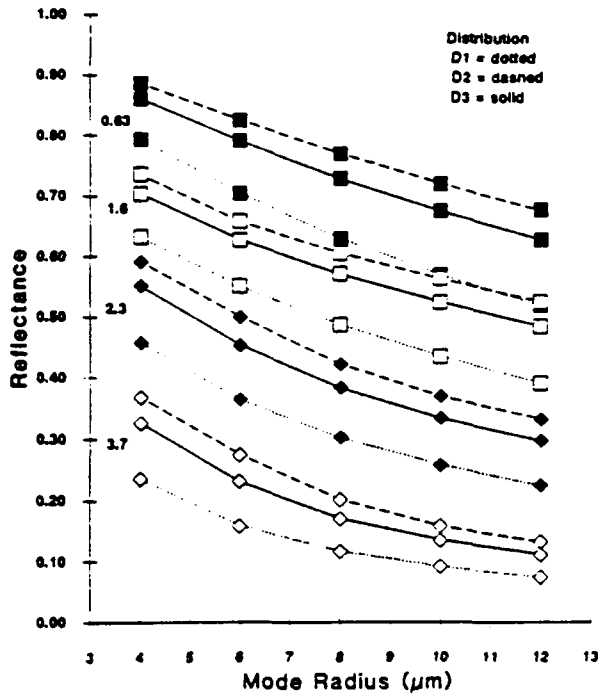


Figure 11. Reflectance vs. Mode Radius.
ELWC = 0.4 gm/m³. Z = 500 m.
θ = 45 degrees.

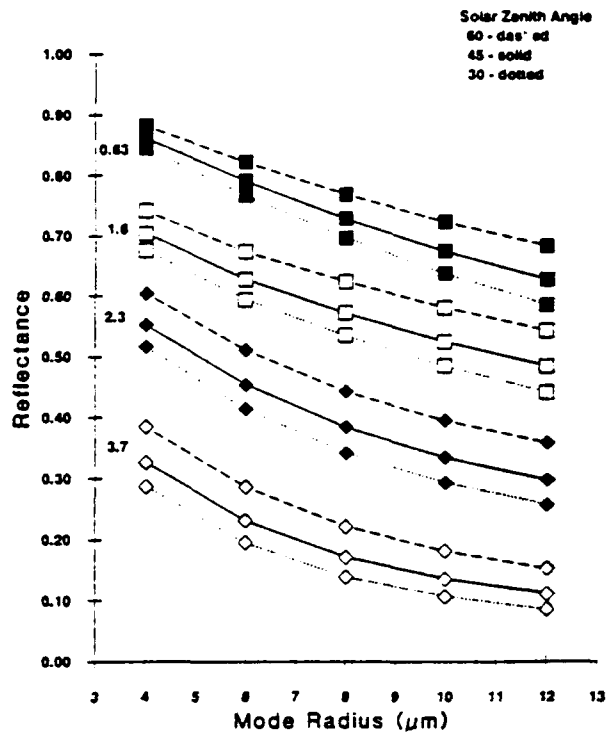


Figure 12. Reflectance vs. Mode Radius.
ELWC = 0.4 gm/m³.
Z = 500 m. D3.

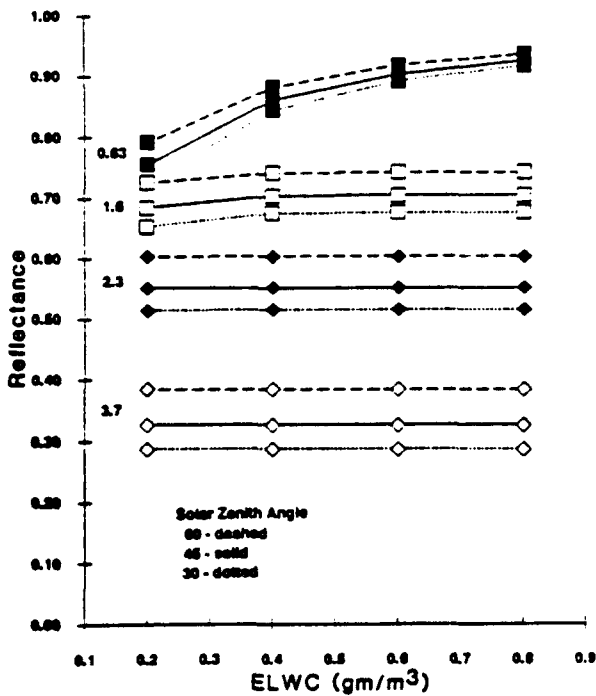


Figure 13. Reflectance vs. ELWC.
Radius = 4.0 μm
Z = 500 m. D3.

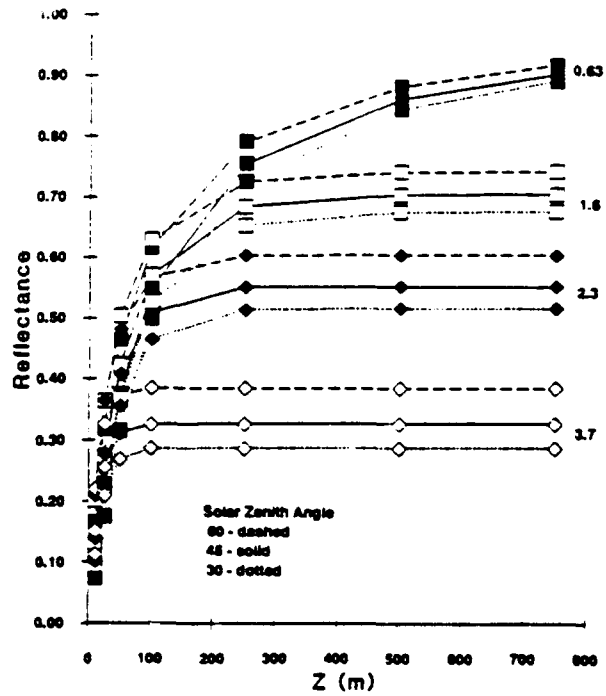


Figure 14. Reflectance vs. Z.
ELWC = 0.4 gm/m³.
Radius = 4.0 μm. D3.

reflectance on distribution, assuming the same mode radius and ELWC, essentially is because more and smaller droplets have higher reflectance.

5.9 Dependence of Reflectance on Solar Zenith Angle

Figures 12 through 14 show that reflectance increases as solar zenith angle increases over the range considered, and that this effect seems to be proportionally more pronounced for the longer wavelengths. The first point can be explained by the strong forward scattering characteristic of this Mie size range. Increasing *sza* allows more scattering into the upper hemisphere. The second point is mainly because for the longer wavelengths the scattered radiation is more anisotropic since it sees a thinner layer of the cloud due to the greater absorption at longer wavelengths.

6. CONCLUSIONS, FUTURE WORK

6.1 Conclusions

The calculated reflectance values depend on a number of different variables, not all independent. Some of the dependencies are simple, while others are more complicated. For example, the complex nature of the index of refraction as a function of wavelength makes interpretation of the reflectance values in terms of absorption properties of water subject to qualifications. Nonetheless, if only one variable at a time is varied, its effect on reflectance can be determined, at least over the range of values considered here. From the calculations one can then derive the following tendencies:

SUMMARY OF VARIATIONS

<u>VARIABLE</u>	<u>CHANGE</u>	<u>REFLECTANCE</u>
r_c	increase	decrease
wavelength	increase	decrease
thickness	increase	increase
ELWC	increase	increase
sza	increase	increase
width(r_c)	increase	decrease

As implied above, some of these changes do not occur without limit. A few remarks are in order to clarify these dependencies.

1. When conditions combine to give the cloud a sufficiently large optical depth (essentially infinite), then any change that acts to increase optical depth has little effect on reflectance. For example, increasing thickness or ELWC beyond certain limits no longer affects reflectance.

2. For a given wavelength and solar zenith angle, the critical cloud factors determining reflectance are single scattering albedo, asymmetry factor, and optical depth. As wavelength varies, the values of these factors will change and as a consequence their relative importance will change. Thus, an effect which may be dominant for one set of values may not be critical for another set.

3. The importance of the asymmetry factor and the single scattering albedo ultimately depends on the directional properties of Mie scattering, which are determined from the relative size of the scatterers compared to the wavelength of the radiation, and on the wavelength dependence of the complex index of refraction of water.

4. If ELWC is kept constant, then decreasing the effective radius of the droplets results in more and smaller droplets which increase reflectance. This is relevant to the ship track phenomenon, as discussed below.

5. Switching to a longer wavelength reduces the reflectance in general because of increased absorption. Note that this is based on the results for four wavelengths. Because of the undulatory nature of the imaginary part of the index of refraction, this observation may not apply at all wavelengths.

6. Subject to the qualification discussed in point 1, an increase in ELWC will increase reflectance until optical depth saturates. A similar conclusion holds for cloud thickness. Larger particles require a larger value of ELWC for optical depth to saturate, i.e., for reflectance to become insensitive to further increase in ELWC. Similarly, for larger particles a larger thickness is required for reflectance to saturate. The reasons for this were discussed in Section 5.2.

7. Variations in solar zenith angle have a larger effect on reflectance for longer wavelengths.

8. Effects of distribution can be explained mainly in terms of differing effective radius, as mentioned in point 4.

From the above results two general recommendations can be made regarding wavelength selection for determining cloud conditions:

1. The shorter wavelengths (e.g., $.63 \mu\text{m}$) are more useful for determining cloud thickness because the longer wavelengths see a thinner layer of the cloud due to absorption limitations.

2. On the other hand, the longer wavelengths are more sensitive to the cloud microphysics, such as droplet size and ELWC. Since for NIR solar radiation, incident energy drops off with increasing wavelength and reflectance decreases at the longer wavelengths, then the shortest wavelength that remains sensitive to cloud microphysics should be used. This has the advantage of increasing receiver sensitivity. Mineart had previously shown that $3.7 \mu\text{m}$ was a possible candidate. The current work suggests that 1.6 or $2.3 \mu\text{m}$ might also be useful choices, especially if several such channels can be used together. Taken together several VIS and NIR channels can be used to provide measures of both cloud geometry (thickness) and microphysics (mode radius and ELWC). For example, a shorter wavelength could be used to estimate cloud thickness, and then the shortest wavelength unaffected by cloud thickness could be used to

estimate microphysics. In combination with other data or other satellite sensor information, these reflectance measurements could provide even more accurate estimates.

Finally, with respect to ship tracks specifically, the results above should have some applicability. The tracks are quite wide, typically a few to twenty kilometers, compared to their depth, typically some fraction of a kilometer (the thickness of marine stratus and stratocumulus clouds). Thus, the assumption of an infinite plane parallel atmosphere is not so bad. Furthermore, for these kinds of clouds, changes in reflectance are probably mostly due to changes in droplet size because of saturation effects in the other possible causes, such as ELWC and cloud thickness. The model results show that reflectance as droplet size decreases will increase at both $.63 \mu\text{m}$ and $3.7 \mu\text{m}$, but that percentage-wise, this effect is more pronounced at the longer wavelength. This is consistent with AVHRR images of ship tracks in channels 1 and 3. Figure 15 is approximately the same scene as in Figure 1, but it includes radiance scans across the tracks, indicating in a more quantitative way how the radiance is enhanced across the track. It should be noted that channel 3 radiance includes both solar reflectance and thermal emittance. When this thermal component is removed (by estimating the Planck temperature from channel 4 ($11 \mu\text{m}$)), the resulting image is usually very similar to the channel 3 image, and so is also in agreement with the model results. It should also be remembered that the model calculates hemispheric reflectance, whereas the AVHRR images depend upon sun-scene-satellite geometry.

6.2 Future Work

6.2.1 N-layer model

Real clouds have differing droplet number concentrations from base to top. If the wavelengths of interest are short enough to "see" several such layers, then a simple one-layer model may not be accurate enough. Codes for simple n-layer models are readily available and should be tried for problems such as cloud models with an evaporation layer on top.

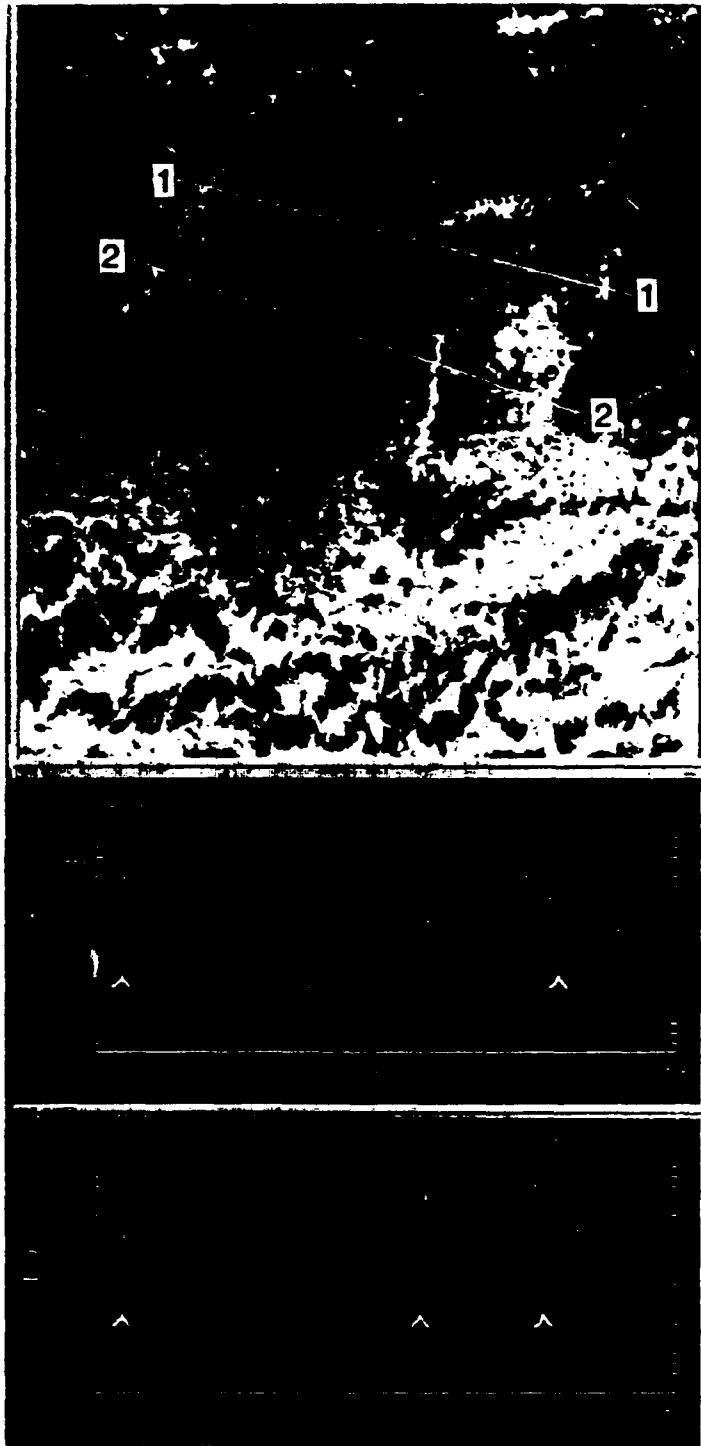


Figure 15. Channel 3 scans across ship tracks in the eastern North Atlantic. DTG is 890512 14:40 GMT. The scene is approximately the same as for Figure 1.

6.2.2 Multi-channel correlations

Even for the simple model used for this report much of the data base remains unexamined because of its size. Because the data is in tabular form, it should be straightforward to use a database management system to look for other variable dependencies, especially involving several channels simultaneously. This offers the advantage of determining some parameter in several different ways, thus improving its accuracy.

6.2.3 Nonhomogeneous finite clouds

Real clouds are generally finite in lateral extent, introducing the problem of side effects, with horizontal composition inhomogeneities. To model such clouds requires much more complicated programs. To the extent that it is possible, keeping a model as simple as possible is desirable, since it makes cause and effect analysis much easier.

6.2.4 Polarization effects

In this study unpolarized radiation was assumed. It would be interesting to investigate if any parameters have a polarization sensitivity.

6.2.5 Comparison with field data - satellite, aircraft

The ultimate test of model-based conclusions is comparison with field data. For the case of cloud reflectances, this means in situ measurements of cloud properties like thickness, droplet number densities, and ELWC, and concurrent satellite measured reflectances. Some data is available from past field experiments such as FIRE and relevant planned experiments, such as a component of ASTEX, should provide additional data.

REFERENCES

- Coakley, Jr., J.A., R.L. Bernstein, and P.A. Durkee (1987). Effect of ship stack effluents on cloud reflectivity. Science 237:1020-1022.
- Deirmendjian, D. (1969). Electromagnetic Scattering on Spherical Polydispersions. New York, Elsevier, 290 pp.
- Hansen, J. E. and L. D. Travis (1974). Light scattering in planetary atmospheres. Space Sci. Rev. 16:527-610.
- Joseph, J. H., W. J. Wiscombe, and J. A. Weinman (1976). The delta-Eddington approximation for radiative flux transfer. J. Atmos. Sci. 33:2452-2459.
- Kerker, M. (1969). The Scattering of Light and Other Electromagnetic Radiation. New York, Academic Press, 666 pp.
- Liou, K.-N., (1980). An Introduction to Atmospheric Radiation. New York, Academic Press, 392 pp.
- Mineart, G., (1988). Multispectral Satellite Analysis of Marine Stratocumulus Cloud Microphysics. M.S. thesis, Naval Postgraduate School, Monterey, CA.
- Shettle, E. P. and J. A. Weinman (1970). The transfer of solar irradiance through inhomogeneous turbid atmospheres evaluated by Eddington's approximation. J. Atmos. Sci. 27:1048-1055.
- Siquig, R.A., A.P. Kuciauskas, and N. Khazenie (1991). Using Clouds to Track Surface Ships. Presented at Cloud Impacts on DoD Operations and Systems 1991 Conference (CIDOS-91), El Segundo, CA, July.
- Wiscombe, W. J. (1980). Improved Mie scattering algorithms. Applied Optics 19:1505-1509.

DISTRIBUTION LIST

ASST. SEC. OF THE NAVY
ATTN: SCIENCE OFFICER
RSCH. ENG. & SYSTEMS
WASHINGTON, DC 20350-1000

CHIEF OF NAVAL OPERATIONS
ATTN: OP-096, OP-0961B
U.S. NAVAL OBSERVATORY
WASHINGTON, DC 20392-1800

SPAWARSSYSCOM
ATTN: PMW 141
WASHINGTON, DC 20363-5100

NOARL
ATTN: CODE 100
JCSSC, MS 39529-5004

NOARL
ATTN: CODE 125L (10)
JCSSC, MS 39529-5004

NOARL
ATTN: CODE 125P
JCSSC, MS 39529-5004

NOARL
ATTN: CODE 104
JCSSC, MS 39529-5004

NOARL
ATTN: CODE 300
JCSSC, MS 39529-5004

DIRECTOR OF NAVY LABORATORIES
CRYSTAL PLAZA BLDG. 5
DEPT. OF THE NAVY
WASHINGTON, DC 20360

UNIVERSITY OF CALIFORNIA
SCRIPPS INST. OF OCEANOGRAPHY
BOX 6049
SAN DIEGO, CA 92106

OFFICE OF NAVAL TECHNOLOGY
ATTN: DR. P. SELWYN, CODE 20
800 N. QUINCY ST.
ARLINGTON, VA 22217-5000

OFFICE OF NAVAL RESEARCH
ATTN: CODE 12
800 N. QUINCY ST.
ARLINGTON, VA 22217-5000

COMMANDER IN CHIEF
U.S. ATLANTIC FLEET
ATTN: FLT METEOROLOGIST
NORFOLK, VA 23511-5210

COMMANDER IN CHIEF
U.S. ATLANTIC FLEET
ATTN: NSAP SCIENCE ADVISOR
NORFOLK, VA 23511-5210

CINCPACFLT
ATTN: CODE O2M
PEARL HARBOR, HI 96860-7000

CINCUSNAVEUR
BOX N39
FPO AE 09510-0150

ASST. SEC. OF THE NAVY (R&D)
ATTN: ASST. FOR ENV. SCI.
ROOM 5E731, THE PENTAGON
WASHINGTON, DC 20350

OFFICE OF NAVAL RESEARCH
ATTN: CODE 1122AT
ARLINGTON, VA 22217-5000

OFFICE OF NAVAL RESEARCH
ATTN: HEAD, OCEAN SCIENCES DIV
CODE 1122
ARLINGTON, VA 22217-5000

OFFICE OF NAVAL RESEARCH
ATTN: CODE 1122 MM, MARINE MET
ARLINGTON, VA 22217-5000

OFFICE OF NAVAL TECHNOLOGY
ATTN: CODE 22
800 N. QUINCY ST.
ARLINGTON, VA 22217-5000

NATIONAL SECURITY AGENCY
ATTN: LIBRARY (2C029)
FT. MEADE, MD 20755

J-3/ESD JOINT STAFF
ATTN: OPERATIONS DIRECTORATE
WASHINGTON, DC 20318-3000

CENTER FOR NAVAL ANALYSES
4401 FORT AVE.
P.O. BOX 16268
ALEXANDRIA, VA 22302-0268

NOARL
ATTN: A. PRESSMAN, CODE 321
JCSSC, MS 39529-5004

COMMANDING OFFICER
FLEET INTELLIGENCE CENTER
(EUROPE & ATLANTIC)
NORFOLK, VI 23522

COMMANDING OFFICER
FLEET INTELLIGENCE CENTER
(PACIFIC)
PEARL HARBOR, HI 96860

U.S. NAVAL ACADEMY
ATTN: LIBRARY REPORTS
ANNAPOLIS, MD 21402

U.S. NAVAL ACADEMY
ATTN: OCEANOGRAPHY DEPT.
ANNAPOLIS, MD 21402

SPAWARSYSCOM
ATTN: CODE 312
NAT. CTR. #1
WASHINGTON, DC 20363-5100

AFGL/LY
ATTN: MET. OFFICER
HANSCOM AFB, MA 01731

USAFETAC/TS
ATTN: TECH. LIBRARY
SCOTT AFB, IL 62225

COMMANDING OFFICER
U.S. ARMY RESEARCH OFFICE
ATTN: GEOPHYSICS DIV.
P.O. BOX 12211
RESEARCH TRIANGLE PARK, NC
27709

DIRECTOR, ENV. & LIFE SCI.
OFFICE OF UNDERSECRETARY OF
DEFENSE FOR RSCH & ENG E&LS
RM. 3D129, THE PENTAGON
WASHINGTON, DC 20505

CENTRAL INTELLIGENCE AGENCY
ATTN: OCR STANDARD DIST.
WASHINGTON, DC 20505

DIRECTOR, TECH. INFORMATION
DEFENSE ADV. RSCH PROJECTS
1400 WILSON BLVD.
ARLINGTON, VA 22209

COMMANDING OFFICER
USCG RSCH & DEV. CENTER
GROTON, CT 06340

DIRECTOR
NATIONAL EARTH SAT. SERV/SEL
FB-4, S321B
SUITLAND, MD 20233

CHIEF
MARINE & EARTH SCI. LIBRARY
NOAA, DEPT. OF COMMERCE
ROCKVILLE, MD 20852

OCEANOGRAPHIC SERVICES DIV.
NOAA
6010 EXECUTIVE BLVD.
ROCKVILLE, MD 20852

REPORT DOCUMENTATION PAGE

Form Approved
OBM No. 0704-0188

Public reporting burden for this collection of information is estimated to average 1 hour per response, including the time for reviewing instructions, searching existing data sources, gathering and maintaining the data needed, and completing and reviewing the collection of information. Send comments regarding this burden or any other aspect of this collection of information, including suggestions for reducing this burden, to Washington Headquarters Services, Directorate for Information Operations and Reports, 1215 Jefferson Davis Highway, Suite 1204, Arlington, VA 22202-4302, and to the Office of Management and Budget, Paperwork Reduction Project (0704-0188), Washington, DC 20503.

1. Agency Use Only (Leave blank).	2. Report Date. November 1991	3. Report Type and Dates Covered. Final	
4. Title and Subtitle. A Simple Cloud Reflectance Model for Ship Tracks in Clouds		5. Funding Numbers. Program Element No. 62435N Project No. RM35G87 Task No. 1 Accession No. DN656774 Work Unit No. 6.2-22	
6. Author(s). Richard A. Siquig		8. Performing Organization Report Number. NOARL Technical Note 175	
7. Performing Organization Name(s) and Address(es). Naval Oceanographic and Atmospheric Research Laboratory Atmospheric Directorate Monterey, CA 93943-5006		10. Sponsoring/Monitoring Agency Report Number. NOARL Technical Note 175	
9. Sponsoring/Monitoring Agency Name(s) and Address(es). Office of Naval Technology (Code 22) 800 N. Quincy St. Arlington, VA 22217-5100			
11. Supplementary Notes.			
12a. Distribution/Availability Statement. Approved for public release; distribution is unlimited.		12b. Distribution Code.	
13. Abstract (Maximum 200 words). Under certain meteorological conditions ships may generate "tracks" in overlying marine stratus or stratocumulus clouds. These tracks are often not particularly evident to satellite sensors at visible wavelengths, but show up much more clearly at near-infrared wavelengths, such as channel 3 (3.7 micrometers) of the Advanced Very High Resolution Radiometer (AVHRR) on NOAA polar-orbiting satellites. This phenomenon represents a potential naval intelligence technique, not only as a means to monitor and perhaps classify ships of other nations but also as a measure of environmental vulnerability of U.S. ships. A simple theoretical model was used as a part of a ship track study to investigate effects of changes in microphysics and geometry on cloud reflectance at certain solar wavelengths. The model assumed a plane parallel homogeneous atmosphere of infinite extent and finite thickness, with Mie scattering and the delta-Eddington approximation for radiative transfer. The results were consistent with the theory that ship exhaust can increase the number density of smaller cloud droplets, which would lead to an increase in reflectance of incident solar radiation, especially at wavelengths near 3.7 micrometers.			
14. Subject Terms. Cloud reflectance Cloud microphysics		AVHRR Ship tracks	15. Number of Pages. 38
			16. Price Code.
17. Security Classification of Report. UNCLASSIFIED	18. Security Classification of This Page. UNCLASSIFIED	19. Security Classification of Abstract. UNCLASSIFIED	20. Limitation of Abstract. Same as report